Physics Letters B 751 (2015) 371–375

Contents lists available at ScienceDirect

Physics Letters B

www.elsevier.com/locate/physletb

# Observation of isoscalar multipole strengths in exotic doubly-magic $^{56}$Ni in inelastic $\alpha$ scattering in inverse kinematics

S. Bagchi [a,*], J. Gibelin [b], M.N. Harakeh [a], N. Kalantar-Nayestanaki [a], N.L. Achouri [b], H. Akimune [c], B. Bastin [d], K. Boretzky [e], H. Bouzomita [d], M. Caamaño [f], L. Càceres [d], S. Damoy [d], F. Delaunay [b], B. Fernández-Domínguez [f], M. Fujiwara [g], U. Garg [h], G.F. Grinyer [d], O. Kamalou [d], E. Khan [i], A. Krasznahorkay [j], G. Lhoutellier [b], J.F. Libin [d], S. Lukyanov [k], K. Mazurek [l], M.A. Najafi [a], J. Pancin [d], Y. Penionzhkevich [k,m], L. Perrot [i], R. Raabe [n], C. Rigollet [a], T. Roger [d], S. Sambi [n], H. Savajols [d], M. Senoville [b], C. Stodel [d], L. Suen [d], J.C. Thomas [d], M. Vandebrouck [b,d,i], J. Van de Walle [a]

[a] KVI-CART, University of Groningen, NL-9747 AA, Groningen, The Netherlands
[b] LPC Caen, ENSICAEN, Université de Caen, CNRS/IN2P3, Caen, France
[c] Department of Physics, Konan University, Kobe 568-8501, Japan
[d] Grand Accélérateur National d'Ions Lourds (GANIL), CEA/DSM-CNRS/IN2P3, Bvd Henri Becquerel, 14076 Caen, France
[e] GSI Helmholtzzentrum für Schwerionenforschung GmbH, 64291 Darmstadt, Germany
[f] Universidade de Santiago de Compostela, E-15706 Santiago de Compostela, Spain
[g] Research Center for Nuclear Physics, Osaka University, Osaka 567-0047, Japan
[h] Physics Department, University of Notre Dame, Notre Dame, IN 46556, USA
[i] Institut de Physique Nucléaire, Université Paris Sud, IN2P3-CNRS, F-91406 Orsay Cedex, France
[j] Institute of Nuclear Research (ATOMKI), Debrecen, P.O. Box 51, H-4001, Hungary
[k] G.N. Flerov Laboratory of Nuclear Reactions, Joint Institute for Nuclear Research, Dubna, Moscow oblast, 144980, Russia
[l] Institute of Nuclear Physics PAN, ul. Radzikowskiego 152, 31-342 Kraków, Poland
[m] National Research Nuclear Center, Moscow Engineering Physics Institute, Kashirskoe sh. 31, Moscow, 115409, Russia
[n] Instituut voor Kern- en Stralingsfysica, KU Leuven, B-3001 Leuven, Belgium

ARTICLE INFO

*Article history:*
Received 8 May 2015
Received in revised form 10 October 2015
Accepted 23 October 2015
Available online 28 October 2015
Editor: V. Metag

ABSTRACT

The Isoscalar Giant Monopole Resonance (ISGMR) and the Isoscalar Giant Dipole Resonance (ISGDR) compression modes have been studied in the doubly-magic unstable nucleus $^{56}$Ni. They were measured by inelastic $\alpha$-particle scattering in inverse kinematics at 50 MeV/u with the MAYA active target at the GANIL facility. The centroid of the ISGMR has been obtained at $E_x = 19.1 \pm 0.5$ MeV. Evidence for the low-lying part of the ISGDR has been found at $E_x = 17.4 \pm 0.7$ MeV. The strength distribution for the dipole mode shows similarity with the prediction from the Hartree–Fock (HF) based random-phase approximation (RPA) [1]. These measurements confirm inelastic $\alpha$-particle scattering as a suitable probe for exciting the ISGMR and the ISGDR modes in radioactive isotopes in inverse kinematics.



Recent developments in nuclear physics involve the studies of short-lived exotic nuclei. New phenomena, such as, neutron halos, neutron skins, and modification of the magic numbers, occur for large neutron-to-proton ($N/Z$) ratios far from stability. The study of collective modes, the so-called giant resonances, in stable nuclei has been one of the important physics motivations throughout the history of nuclear physics. However, very little information about the collective properties of exotic nuclei is available. Among these collective modes, the ISGMR and the ISGDR are of prime interest as their excitation energies are directly related to the incompressibility of a nucleus, $K_A$ [2,3]. The incompressibility of nuclear matter ($K_\infty$) is defined as the curvature of the energy per particle at the saturation density [4], and can be deduced from $K_A$ [4–6]. It is an important key input to the equation of state (EoS) of nuclear matter which, in turn, is useful in understanding some astrophysical quantities, such as, radii and masses of neutron stars, and also in understanding the mechanism of supernovae explosions.

* Corresponding author.
*E-mail address:* soumya.bagchi87@gmail.com (S. Bagchi).

http://dx.doi.org/10.1016/j.physletb.2015.10.060

The value of $K_\infty$ obtained from the ISGMR and the ISGDR data in stable nuclei is $240 \pm 10$ MeV [4,6–8]. Theoretical calculations with effective interactions using this value of $K_\infty$ can reproduce well the centroid energies of the ISGMR for $^{90}$Zr, $^{144}$Sm, and $^{208}$Pb. On the other hand, they overestimate the centroid energies for the ISGMR strength distributions in Sn [9,10] and Cd [11] isotopes, although they can reproduce well the ground-state properties for these isotopes. Nevertheless, the investigation of the ISGMR along the isotopic chains of Cd [11] and Sn [12] helped determine the symmetry energy of the EoS. In spite of significant theoretical efforts to reproduce simultaneously the ISGMR centroid energies in $^{90}$Zr, $^{208}$Pb, and in Sn/Cd isotopes, the problem remains as to why the isotopes of Sn and Cd are soft [9–11]. It should be mentioned that a recent attempt to fit the centroid energies of soft $^{120}$Sn and stiff $^{208}$Pb simultaneously [13,14] yielded a smaller value of $K_\infty$ with a large uncertainty, i.e., $230 \pm 40$ MeV. Therefore, it is useful to study compression modes for another series of isotopes to determine both $K_\infty$ and the symmetry energy parameter of the EoS. Ni isotopes provide such an isotopic series widely ranging over $N/Z$ ratios. Therefore, efforts have been put to study in detail the compression modes for several stable and unstable isotopes of Ni from the neutron-deficient to the neutron-rich regions of the nuclear chart.

Measurements of giant resonances in unstable nuclei are particularly challenging. Up to now such measurements have been mainly performed to study the isovector giant dipole resonance in neutron-rich radioactive oxygen [15], neon [16], and tin [17] isotopes, and in $^{68}$Ni [18]. These studies have been performed through Coulomb excitation by scattering from a Pb target at relativistic energies. On the other hand, the best probe to study the isoscalar modes in a nucleus is either inelastic $\alpha$-particle scattering or inelastic deuteron scattering as both the $\alpha$ particle and deuteron have zero isospin. The isoscalar responses have been so far measured for the unstable doubly-magic $^{56}$Ni nucleus by inelastic deuteron scattering [19] and for the unstable neutron-rich $^{68}$Ni nucleus by inelastic $\alpha$-particle and deuteron scattering [20,21]. In our experiment, we focused on the study of isoscalar responses in $^{56}$Ni via inelastic $\alpha$-particle scattering. The choice was made because of the fact that, the $^{56}$Ni$(\alpha,\alpha')^{56}$Ni$^*$ reaction has higher cross section than the $^{56}$Ni$(d,d')^{56}$Ni$^*$ reaction and the unwanted background due to deuteron breakup can be avoided. Another interesting reason to study the collective modes in $^{56}$Ni is because of the important role $^{56}$Ni plays in the astrophysical scenarios. $^{56}$Ni, a doubly-magic closed-shell nucleus, is one of the waiting point nuclei in the stellar nucleosynthesis and it was found in the ejecta of supernova 1987A [22].

The ISGMR cross section is peaked at 0° in the center-of-mass (CM) frame, which corresponds to the detection of very low-energy recoil $\alpha$ particles in the laboratory frame. To measure the excitation energy ranging from 0 MeV (elastic scattering) to 35 MeV in inverse kinematics, it is necessary to detect the recoil $\alpha$ particles having energies up to 4.5 MeV, which corresponds to 8° CM angle. Detection of such low-energy recoil $\alpha$ particles (including sub-MeV) with a particle telescope would necessitate a very thin target ($\sim$30 μg/cm$^2$) to allow the $\alpha$ particles to emerge from the target and to minimize the straggling. This would consequently require the radioactive ion beam to have an intensity of the order of $5 \times 10^6$ particles/s or above in order to have reasonable yields ($\geq$1000 counts for the ISGMR at 5.5° CM angle for a beam time run of 5 days). Although this is feasible with a storage-ring facility, such as the Experimental Storage Ring (ESR) at GSI [23–25], another alternative is to use an active-target detector. An example of such detector is IKAR [26], developed at GSI, which was used to study the elastic scattering of exotic beams at relativistic energies. Another example is MSTPC [27], built in Japan, for studying fusion reactions and reactions of nuclear-astrophysics interest at low energies. In our experiment, we used the MAYA active-target detector [28]. It is a gas target where the target gas acts also as a detector. In an active target such as MAYA, the target thickness can be increased without severe loss of energy resolution by increasing the gas pressure. In this Letter, we present the results of the first measurement of the isoscalar giant resonances in the doubly-magic $^{56}$Ni investigated with inelastic $\alpha$-particle scattering in inverse kinematics using the MAYA active-target detector.

A secondary beam of $^{56}$Ni at 50 MeV/u was produced at the GANIL facility by the *In-Flight* fragmentation technique. The primary stable beam of $^{58}$Ni at 75 MeV/u impinged on a 525.6 μm thick $^9$Be target located at the entrance of the LISE [29] spectrometer. Two dipole magnets and a 500 μm achromatic degrader were used to purify the secondary beam. The average beam intensity of $^{56}$Ni was of the order of $2 \times 10^4$ particles/s with a purity of about 96%. A plastic scintillator detector, followed by the MAYA detector, was put at the end of the LISE spectrometer. The plastic scintillator was used to count the number of incoming beam particles. The active-target detector MAYA, developed at GANIL, is a time-charge projection chamber with an active volume of $28 \times 25 \times 20$ cm$^3$. In the presence of an electric field applied across the target volume, electrons produced through ionization of the gas by the incident beam or reaction products, drift towards a set of 32 amplification wires that are parallel to the beam direction. For a two-body reaction, the angle of the reaction plane can be determined by the drift time of the electrons towards the amplification wires. The avalanches on the amplification wires induce signals on a matrix of $32 \times 32$ hexagonal pads connected to GASSIPLEX [28] chips. MAYA was filled with 95% helium gas and 5% $CF_4$, which acts here as a quencher since pure helium cannot be used due to sparking. The pressure of the gas-mixture was maintained at 500 mbar. With the effective length of 20 cm, a luminosity of around $5 \times 10^{24}$ cm$^{-2}$ s$^{-1}$ was achieved. An electrostatic mask [30] was placed just below the beam trajectory in MAYA. This electrostatic mask helps in reducing the charges due to the highly-ionizing beam particles in comparison to those induced by the very low-energy recoil $\alpha$ particles, thus effectively increasing the dynamic range for charge-detection.

For each event, two observables are measured to reconstruct the reaction kinematics: the range and the scattering angle of the recoil particle. Since MAYA is a time-charge projection chamber, the projected recoil angle is reconstructed using a "global fitting method" as described in Refs. [20,21,31]. In this method, a straight-line trajectory is obtained by minimizing the orthogonal distances of the centers of the pads weighted by the charges on the pads to the fitted trajectory line. The intersection of the fitted trajectories of the beam path and the recoil-particle path determines the vertex of interaction. From the charge projection of the recoil $\alpha$ particle, the Bragg peak is determined and the projected range of the recoil particle is measured from the vertex of interaction. Recoil particles from the quenching gas were rejected on an event-by-event basis using the total charge integral versus the range of the ionizing particles. The third dimension is obtained from the drift times of the electrons towards the amplification wires. The scattering angle is obtained from the projected angle on the pads and the measured drift times. After obtaining the range in three dimensions, the energy of the recoil $\alpha$ particle is deduced using range-to-energy tables in SRIM [32]. The range, energy, and scattering angle of the recoil particle are deduced on an event-by-event basis. A reliable trajectory reconstruction has been achieved for recoil $\alpha$ particles having energies higher than 600 keV.

The reconstructed three-dimensional scattering of the recoil $\alpha$ particles provides the kinematics for the $^{56}$Ni$(\alpha,\alpha')^{56}$Ni$^*$ reaction as presented in Fig. 1, where the energy of the recoil $\alpha$ particle is shown as function of the scattering angle for all events. The solid

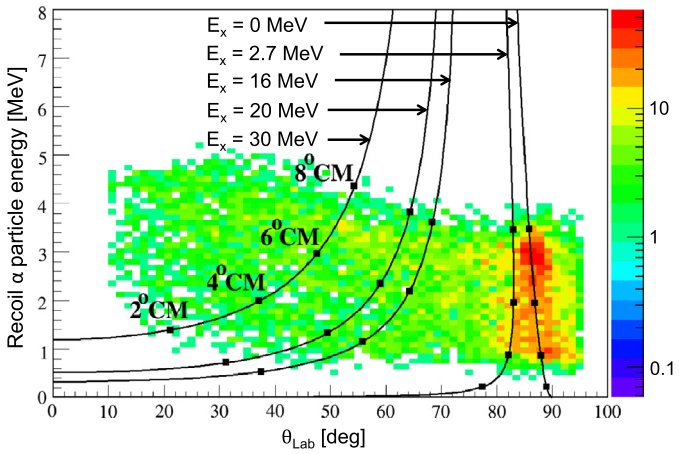


**Fig. 1.** (Color online.) Scatter plot of the kinetic energy versus the scattering angle, reconstructed for the recoil $\alpha$ particles, is shown. The solid lines represent the LISE++ kinematics [33] calculations obtained for $E_x = 0$ MeV (elastic scattering), 2.7 MeV (first-excited state), 16 MeV, 20 MeV, and 30 MeV of $^{56}$Ni. Several CM angles are depicted on the kinematics lines.

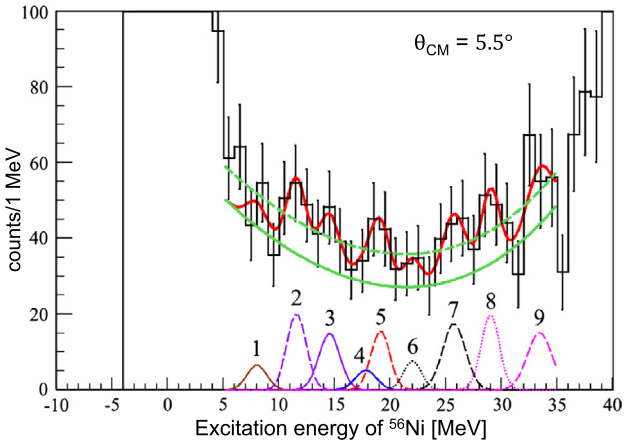


**Fig. 2.** (Color online.) Excitation-energy spectrum of $^{56}$Ni for a 1° bin centered around 5.5° $\theta_{CM}$ angle is shown. The green dashed line represents the background fit to the excitation-energy spectrum assuming no giant-resonance structures. The red solid line is the result of the fit to the data with nine Gaussian peaks and a fitted background. The green solid line represents the final background in the total fit. The nine Gaussian peaks are shown separately with the brown solid line, purple dashed line, purple solid line, blue solid line, red dashed line, black dotted line, black dashed line, magenta dotted line, and magenta dashed line, identified as peaks #1, 2, 3, 4, 5, 6, 7, 8, and 9, respectively. Peak #1 shows an $L = 1$ behavior whereas, peaks #2 and 3 show an $L = 2$ behavior. Peaks #4 and 5 show $L = 1$ and $L = 0$ behaviors, respectively. Peaks #6 to 9 include $L = 1$ mode and higher multipoles.

lines show the kinematics curves for $E_x = 0$ MeV (elastic scattering), 2.7 MeV (first-excited state of $^{56}$Ni), 16 MeV, 20 MeV, and 30 MeV of $^{56}$Ni.

Data are transformed into the CM frame using two-body relativistic kinematics, and are corrected for geometrical and reconstruction efficiencies along with detector acceptances. These efficiencies are deduced from simulations having inputs from LISE++ kinematics [33] and SRIM [32] outputs; details are given in Ref. [34]. The peak around $E_x = 0$ MeV corresponds to elastic scattering and the first-excited state of $^{56}$Ni. The full width at half maximum (FWHM) of this "elastic-scattering" peak is around 4.5 MeV. The broadening of this peak is due to trajectory reconstruction of low-energy recoil $\alpha$ particles and due to the presence of low-lying states mainly the $2^+$ state which is situated at $E_x = 2.7$ MeV [35]. In this context, it is worthwhile to mention the detector resolution for different excitation energies, obtained from simulations [34]. The detector resolutions (FWHM) for $E_x = 0$ MeV, 10 MeV, 20 MeV, 30 MeV, and 40 MeV are obtained to be 2.24 MeV, 2.16 MeV, 1.90 MeV, 1.38 MeV, and 1.23 MeV, respectively. It is, therefore, clear that as the excitation energy increases, the resolution of the detector improves. This is due to the fact that with the increase of excitation energy, the energy of the recoil $\alpha$ particle increases for a given CM angle (as can be seen from the kinematics lines in Fig. 1) which leads to better trajectory reconstruction of the recoil products in MAYA. Six excitation-energy spectra are obtained for the angular bins 3°–4°, 4°–5°, 5°–6°, 6°–7°, 7°–8°, and 8°–9°. Fig. 2 displays the excitation-energy spectrum for a 1° bin centered around 5.5° CM angle. The fact that there are several peaks in the excitation-energy range between 5 MeV to 35 MeV points to the presence of several fragmented isoscalar modes.

The data analysis is first performed by fitting the excitation-energy spectra for the different CM angles below 9°. Inspection of the spectra showed that at certain angles some peaks are prominent resulting in a total of nine peaks being prominent at different angles for the excitation-energy range 5–35 MeV. Therefore, a 9-peak fit is performed for all excitation-energy spectra using Gaussian functions. This large number of fragments of the multipole strength has been previously observed in this mass region [36,37,39]. The background shape is obtained by first fitting the excitation-energy spectra between 5 MeV and 35 MeV with a polynomial of order 4 assuming no giant-resonance structures in the spectra. Concerning the background shape, we have decided on a polynomial of order 4 because of the following. Simulations for the elastic scattering peak showed a tail that extended to higher excitation energy, resulting from the misidentification of elastic scattering events because of their very short tracks in MAYA. On the other hand, experiments on stable nuclei show a physical background at higher energies due mainly to the quasi-elastic knockout reaction, which starts at the particle separation threshold and increases to almost a constant at very high excitation energies. The sum of these two backgrounds justifies the use of a background with a trough shape with a broad minimum around 20 MeV. In the total fit of the excitation-energy spectra for a given CM angle, i.e., nine Gaussian functions and the background, the obtained background shape is then kept fixed. An extra additive parameter, used to determine the height of the background, is kept free. The width of a Gaussian fitting an observed giant-resonance structure is varied in the fit for the CM angle where the corresponding structure is the most prominent. After obtaining the width parameter in this manner, it has been kept fixed for other CM angles where the corresponding structure height is less pronounced. Data up to 35 MeV excitation energy have been considered, above which data are neglected because they suffer from the low-acceptance of the detector. Due to the uncertainty in subtracting the background, possible contributions from the continuum due to knock-out reactions could also be present at these high energies.

Comparing angular distributions of peaks obtained with this method with results from the calculations using distorted-wave Born approximation (DWBA) (see below), peaks #2 and 3 in Fig. 2 with centroid positions at $E_x = 11.0 \pm 0.5$ MeV and $14.4 \pm 0.5$ MeV, respectively, were found to have angular distributions characteristic of quadrupole ($L = 2$) transitions (see Fig. 3). The corresponding FWHMs were measured to be $2.0 \pm 0.3$ MeV and $2.2 \pm 0.2$ MeV, respectively. From the quasi-particle RPA with a Skyrme interaction (SkM*) [38], it can be seen that there exists a low-lying isoscalar dipole mode ($L = 1$) around 16–17 MeV. Evidence for this low-lying dipole mode was found in the present analysis (peak #4 in Fig. 2) with the centroid position at $E_x = 17.4 \pm 0.7$ MeV. The monopole mode (peak #5 in Fig. 2) was also identified at $E_x = 19.1 \pm 0.5$ MeV. A FWHM of $2.0 \pm 0.3$ MeV was extracted

**Table 1**
Centroids of the ISGMR and the low-lying component of the ISGDR in $^{56}$Ni and $^{58}$Ni [39] obtained from inelastic $\alpha$-particle scattering. The result obtained for the ISGMR in $^{56}$Ni with inelastic deuteron scattering [19] is also shown. The centroid values listed in the table are obtained from the peak fitting in the excitation-energy spectra.

| | ISGMR $E_x$ [MeV] | Low-lying component of ISGDR $E_x$ [MeV] |
|---|---|---|
| $^{56}$Ni$(\alpha,\alpha')$ (This work) | $19.1 \pm 0.5$ | $17.4 \pm 0.7$ |
| $^{56}$Ni$(d,d')$ [19] | 19.5 | |
| $^{58}$Ni$(\alpha,\alpha')$ [39] | $18.43 \pm 0.15$ | $17.42 \pm 0.25$ |

**Table 2**
Optical-model parameters used in the DWBA calculations.

| Nucleus | $E_\alpha$ [MeV] | $V_{Real}$ [MeV] | $V_{Imag}$ [MeV] | $r_{Real}$ [fm] | $r_{Imag}$ [fm] | $a_{Real}$ [fm] | $a_{Imag}$ [fm] | $r_C$ [fm] |
|---|---|---|---|---|---|---|---|---|
| $^{58}$Ni [41] | 240 | 76.6 | 24.2 | 1.242 | 1.435 | 0.8 | 0.8 | 1.3 |

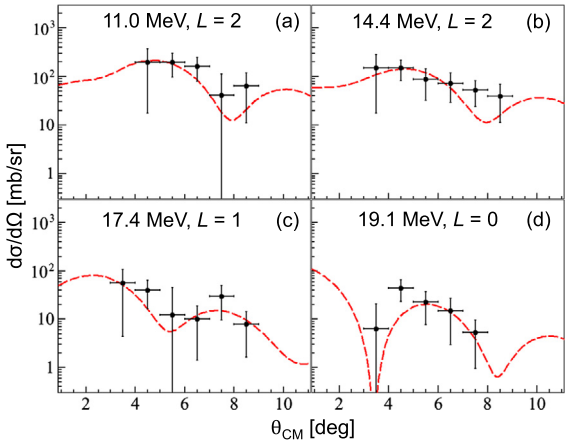


**Fig. 3.** (Color online.) Experimental angular distributions for the peaks located at 11.0 MeV (a), 14.4 MeV (b), 17.4 MeV (c), and 19.1 MeV (d) are shown as black data points with error bars. The red dashed lines show the DWBA predictions for isoscalar resonances with multipoles $L = 2$ (a) and (b), $L = 1$ (c) and $L = 0$ (d).

here. This rather small value compared to those of neighboring nuclei [39], is probably due to the low statistics and small signal-to-noise ratio. Errors on the centroid positions and the widths of different modes are obtained from the fitting of the peaks in the excitation-energy spectra with Gaussian functions. The centroid positions of the monopole mode and the low-lying dipole mode obtained from this work are compared with other works [19,39] in Table 1.

The angular distributions of the Gaussian peaks #2, 3, 4, and 5 in Fig. 2 are shown in Fig. 3. Error bars of the data are the square roots of the quadratic sums of errors due to statistical fluctuations, errors due to efficiency calculations, and errors in the background heights. These angular distributions are well reproduced by the DWBA calculations assuming $L = 2$, 2, 1, and 0 multipolarities, respectively. The theoretical calculations were performed using the code CHUCK3 [40]. The optical-potential parameters (listed in Table 2) were obtained by fitting the $^{58}$Ni$(\alpha,\alpha)$ elastic scattering data and $^{58}$Ni$(\alpha,\alpha')$ inelastic scattering data of the first-excited state of $^{58}$Ni at 60 MeV/u beam energy [41]. Transition potentials are obtained from collective transition densities following the procedures described in Refs. [42,43].

Another independent analysis was performed using the multipole-decomposition analysis (MDA) method to check the consistency of the results. After background subtraction as described in the Gaussian peak-fitting method, the data were binned in 2 MeV to improve the statistics. Angular distributions were obtained for

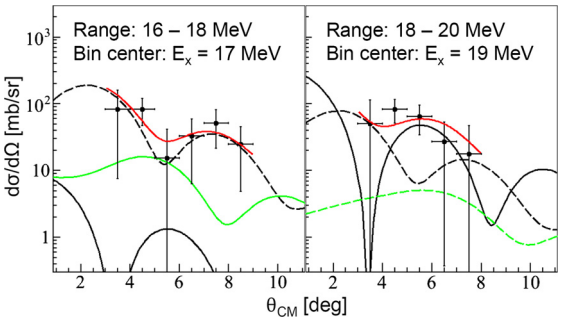


**Fig. 4.** (Color online.) MDA fittings of the experimental cross sections (black data points with error bars) are shown for two excitation-energy ranges; 16 MeV to 18 MeV (left panel) and 18 MeV to 20 MeV (right panel). Angular distributions with the black solid line, the black dashed line, the green solid line, and the green dashed line are obtained for $L = 0$, $L = 1$, $L = 2$, and $L = 3$ multipoles, respectively, from DWBA calculations using collective transition potentials (see text) and the optical-potential parameters listed in Table 2. The calculations are performed at the excitation energy corresponding to the bin center of a given bin having size of 2 MeV. The red solid lines represent the fits to the data.

the excitation energies ranging from 9 MeV to 35 MeV with 2 MeV energy bins and were fitted using a linear combination of theoretical angular distributions of multipolarities $L = 0$, $L = 1$, $L = 2$, and $L = 3$. Since MAYA is phase-space limited because of the limitations in detecting the very low- and high-energy recoil $\alpha$ particles, the number of data points in the angular distributions is also limited from 3° to 8° CM angle. Hence, the multipoles which are relevant at a given excitation-energy interval have been considered in the fitting instead of considering the contributions of all multipoles at all excitation-energy intervals. Theoretical angular distributions were obtained from the DWBA calculations as described before using the optical-potential parameters listed in Table 2. From MDA, it has been found that the monopole mode has a significant contribution in the excitation-energy region from 18 MeV to 20 MeV (see the right panel of Fig. 4) with the centroid value of the strength distribution measured at $E_x = 18.4 \pm 1.8$ MeV and with a root-mean-square width of $2.0 \pm 1.2$ MeV. The position of the monopole mode obtained from the Gaussian peak-fitting method ($19.1 \pm 0.5$ MeV) and the MDA are in good agreement with each other. Furthermore, the excitation energy of the monopole mode in $^{56}$Ni is also consistent with the value $E_x = 19.3 \pm 0.5$ MeV which is obtained from inelastic deuteron scattering off $^{56}$Ni [19].

Below 15 MeV, there is evidence for the existence of both $L = 1$ and $L = 2$ modes. Like in the Gaussian peak-fitting method, evidence for the low-lying $L = 1$ mode has also been found in the MDA at an excitation energy of around 17 MeV (see the left panel of Fig. 4). According to Refs. [39,44], there is evidence for a low-lying dipole mode in $^{58}$Ni around 16–17 MeV which is higher than the $1\hbar\omega$ component of the ISGDR. Surprisingly, Monrozeau et al. [19] did not observe any isoscalar dipole strength at this energy nor at any other energy in $^{56}$Ni. This is consistent with a *bi-modal* nature of the ISGDR with the centroid of the high-energy component appearing around 30 MeV. Inelastic electron scattering from $^{58}$Ni has been measured by Klein et al. [45]. Unfortunately, in electron scattering it is not possible to disentangle either isoscalar E0 and E2, or isoscalar E1 and E3. However, the structures observed are not in disagreement with results from inelastic $\alpha$ scattering depending on the multipolarity assumed.

To get a qualitative understanding of the ISGDR strength distribution, it has been compared with the predictions of the HF-based RPA calculations [1]. They are shown in Fig. 5 in red solid line. The distribution of the experimental strength, obtained from the MDA, seems consistent with the theoretical prediction but with large errors. Since in the present analysis, no data have been analyzed

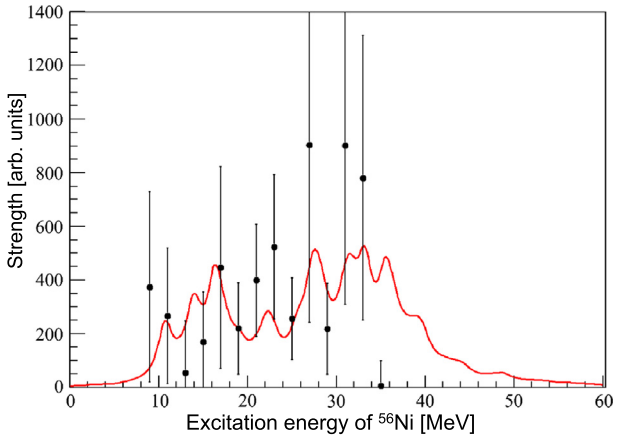


**Fig. 5.** (Color online.) Comparison of the experimental ISGDR strength distribution in $^{56}$Ni (black data points with error bars), obtained from the MDA, is shown together with the prediction of a recent HF-RPA calculation (red solid line) [1].

above 35 MeV, there are no data points shown above 35 MeV in Fig. 5. Due to non-negligible uncertainties in determining the background level and the poor statistics of the data, there are large uncertainties in obtaining the absolute values of the exhausted fractions of the energy-weighted sum rules (EWSR) in the MDA analysis. Both the MDA and the direct comparison of the cross-section angular distribution with theory could, in principle, give us the strength exhausted by a giant-resonance mode. The number we obtain for $L = 0$ is $240 \pm 120\%$, which is, within the errors, in agreement with the value $136 \pm 27\%$ obtained by Monrozeau et al. [19]. Due to strong uncertainties in the normalization associated with measurements with available active targets such as MAYA, as observed here for the elastic scattering data, we cannot give at present a more reliable number. As mentioned earlier, error bars of the data include statistical fluctuations, errors due to efficiency calculations, and errors in the background heights.

To summarize, inelastic $\alpha$-particle scattering off the $^{56}$Ni nucleus has been measured in inverse kinematics using the MAYA active-target detector with an average beam intensity of the order of $2 \times 10^4$ particles/s. The centroid position of the ISGMR has been found to be at $E_x = 19.1 \pm 0.5$ MeV. A low-lying component of the ISGDR has also been found around 17 MeV. This is the first measurement of the compression modes in a neutron-deficient unstable nucleus with inelastic $\alpha$-particle scattering. In spite of the low statistics, the difficulties in background determination, the limitations of our studied energy range to 35 MeV, and the low energy resolution, the present experimental setup is suitable for measuring the properties of unstable and exotic nuclei available at rare-isotope beam facilities worldwide. Efforts are on the way to develop new active-target detectors [46], which will provide access to small-angle measurements with better energy and angular resolution.

## Acknowledgements

This work was supported by the European Commission within the Seventh Framework Programme through IA-ENSAR (contract No. RII3-CT-2010-262010) and GSI Helmholtzzentrum für Schwerionenforschung GmbH, Darmstadt, Germany, and the United States National Science Foundation (Grants Number PHY-1068192 and PHY-1419765).

## References

[1] N. Auerbach, et al., Phys. Rev. C 89 (2014) 014335.
[2] S. Stringari, Phys. Lett. B 108 (1982) 232.
[3] J. Treiner, et al., Nucl. Phys. A 371 (1981) 253.
[4] G. Colò, et al., Phys. Rev. C 70 (2004) 024307.
[5] J.P. Blaizot, et al., Nucl. Phys. A 591 (1995) 435.
[6] B.K. Agrawal, S. Shlomo, V. Kim Au, Phys. Rev. C 68 (2003) 031304(R).
[7] U. Garg, Nucl. Phys. A 731 (2004) 3.
[8] B.G. Todd-Rutel, J. Piekarewicz, Phys. Rev. Lett. 95 (2005) 122501.
[9] J. Piekarewicz, Phys. Rev. C 76 (2007) 031301(R).
[10] U. Garg, et al., Nucl. Phys. A 788 (2007) 36c.
[11] D. Patel, et al., Phys. Lett. B 718 (2012) 447.
[12] T. Li, et al., Phys. Rev. Lett. 99 (2007) 162503.
[13] E. Khan, J. Margueron, I. Vidaña, Phys. Rev. Lett. 109 (2012) 092501.
[14] E. Khan, J. Margueron, Phys. Rev. C 88 (2013) 034319.
[15] A. Leistenschneider, et al., Phys. Rev. Lett. 86 (2001) 5442.
[16] J. Gibelin, et al., Phys. Rev. Lett. 101 (2008) 212503.
[17] P. Adrich, et al., Phys. Rev. Lett. 95 (2005) 132501.
[18] O. Wieland, et al., Phys. Rev. Lett. 102 (2009) 092502.
[19] C. Monrozeau, et al., Phys. Rev. Lett. 100 (2008) 042501.
[20] M. Vandebrouck, et al., Phys. Rev. Lett. 113 (2014) 032504.
[21] M. Vandebrouck, Première mesure des résonances géantes isoscalaires dans un noyau exotique riche en neutrons: le $^{68}$Ni avec la cible active MAYA, Ph.D. thesis, De l'Université Paris Sud, 2013.
[22] H.A. Bethe, Rev. Mod. Phys. 62 (1990) 801.
[23] P. Egelhof, et al., Phys. Scr. T 104 (2003) 151.
[24] M. von Schmid, et al., EPJ Web Conf. 66 (2014) 03093.
[25] J.C. Zamora, et al., Phys. Scr. (2015), accepted.
[26] A.A. Vorobyov, et al., Nucl. Instrum. Methods Phys. Res., Sect. A, Accel. Spectrom. Detect. Assoc. Equip. 270 (1988) 419.
[27] Y. Mizoi, et al., Nucl. Instrum. Methods Phys. Res., Sect. A, Accel. Spectrom. Detect. Assoc. Equip. 431 (1999) 112.
[28] C.E. Demonchy, et al., Nucl. Instrum. Methods Phys. Res., Sect. A, Accel. Spectrom. Detect. Assoc. Equip. 573 (2007) 145.
[29] R. Anne, et al., Nucl. Instrum. Methods Phys. Res., Sect. A, Accel. Spectrom. Detect. Assoc. Equip. 257 (1987) 215.
[30] J. Pancin, et al., J. Instrum. 7 (2012) 01006.
[31] T. Roger, et al., Nucl. Instrum. Methods Phys. Res., Sect. A, Accel. Spectrom. Detect. Assoc. Equip. 638 (2011) 134.
[32] J.F. Ziegler, J. Appl. Phys. 85 (1999) 1249.
[33] LISE++ code, http://lise.nscl.msu.edu/lise.html.
[34] S. Bagchi, Study of compression modes in $^{56}$Ni using an active target, Ph.D. thesis, University of Groningen, 2015.
[35] http://www.nndc.bnl.gov.
[36] D.H. Youngblood, Y.-W. Lui, H.L. Clark, Phys. Rev. C 63 (2001) 067301.
[37] S. Brandenburg, et al., Phys. Lett. B 130 (1983) 9.
[38] J. Terasaki, J. Engel, Phys. Rev. C 74 (2006) 044301.
[39] Y.-W. Lui, et al., Phys. Rev. C 73 (2006) 014314.
[40] J.R. Comfort, M.N. Harakeh, Program CHUCK3, University of Colorado, 1979 (Modified version of CHUCK by P.D. Kunz, unpublished).
[41] H.L. Clark, Y.-W. Lui, D.H. Youngblood, Nucl. Phys. A 589 (1995) 416.
[42] M.N. Harakeh, A. van der Woude, Giant Resonances: Fundamental High-Frequency Modes of Nuclear Excitation, Oxford Studies in Nuclear Physics, Oxford Univ. Press, 2001.
[43] M.N. Harakeh, A.E.L. Dieperink, Phys. Rev. C 23 (1981) 2329.
[44] B.K. Nayak, et al., Phys. Lett. B 637 (2006) 43.
[45] R. Klein, et al., Phys. Lett. B 145 (1984) 25.
[46] J. Pancin, et al., Nucl. Instrum. Methods Phys. Res., Sect. A, Accel. Spectrom. Detect. Assoc. Equip. 735 (2014) 532.